Near Surface Geophysics, 2006, 367-375

2M-SASW: Multifold multichannel seismic inversion of local dispersion of Rayleigh waves in laterally heterogeneous subsurfaces: application to the Super-Sauze earthflow, France

G. Grandjean* and A. Bitri

BRGM, BP 6009, 45060 Orléans, France

Received April 2005, revision accepted March 2006

ABSTRACT

The approach presented here deals with the inversion of Rayleigh wave dispersion (SASW: Spectral Analysis of Surface Waves) in laterally heterogeneous media. The traditional method consists of computing the frequency versus phase-velocity curve, known as the dispersion curve, from seismic records, then inverting to obtain a 1D shear-wave velocity model. When media are laterally heterogeneous, S-wave velocity changes lead to phase variations in Rayleigh waves in the offset dimension. This phenomenon can drastically alter the dispersion image, since it affects the local slopes of Rayleigh waves in the shot gather, and thus their phase-velocity dispersion properties. In the case of multifold acquisitions (2M-SASW: Multifold and Multichannel SASW), we redefine the manner in which the dispersion-image calculation is formulated in order to compute the local dispersion stack (LDS). In principle, this consists of gathering receivers within a restricted window for a series of shots and computing the local dispersion images that are then stacked in order to improve the signal-to-noise ratio. Even though local dispersion diagrams are noisy because they are computed from a limited number of traces, the summation over multiple dispersion images enables the quality of the final LDS to be improved. Because it is related to the dispersion properties of the windowed wavefield, the LDS is an efficient input for the 1D inversion process. The method is tested on synthetic data to demonstrate its contribution compared to that of the traditional SASW technique. An application of the 2M-SASW method to the Super-Sauze earthflow confirms that is well-suited to inverting the shear-wave velocity from Rayleigh-wave dispersion when high-contrast media are considered.

INTRODUCTION

During recent years, spectral analysis of surface waves (SASW) has received increasing attention in the geophysical community (Yaramanci 2004), essentially because it offers a non-invasive means of evaluating the soil shear modulus at depth (O'Neill *et al*. 2003). A wide range of applications have demonstrated the use of this method for geotechnical purposes (Rix *et al*. 2001) and for characterizing lithology, either in land or marine contexts (Bohlen *et al*. 2004). Initial studies on surface-wave analysis were devoted to determining 1D shear-wave velocity structures down to 100 m (Nazarian *et al*. 1983). Most of these studies employed a vibrating source and calculated phase differences between two receivers, using a simple cross-correlation technique.

Later, Park *et al*. (1999a, b) extended the SASW to a multichannel analysis of surface waves (MASW). This method studies Rayleigh-wave dispersion, i.e. the variations of phase velocity with frequency, from a multichannel recording system. The experiment consists of constructing a seismic antenna, composed of a seismic source and several sensors spaced regularly along the seismic line, then recording the soil particle velocity in time after the source has been activated. An integral transformation converts the time-domain waveform data into a phase velocity–frequency domain called the dispersion image. Because the resulting dispersion image is obtained from the stack of several phase-transformed signals recorded by the sensors, aliasing artefacts are reduced, increasing the resolution of the final image. Consequently, this improvement in resolution makes it possible to distinguish each separate propagation mode.

Another extension of the method, developed by Xia *et al*. (1999) and Miller *et al*. (1999), consists of obtaining a 2D shear-wave velocity profile through the shallowest layers (Lin and Chang 2004; Grandjean, in press). A series of consecutive shots are recorded sequentially for different positions of the seismic antenna along the profile. Each seismic record is transformed into a dispersion image (Park *et al*. 1998) from which the fre-

g.grandjean@brgm.fr

quency versus phase-velocity curve, known as the dispersion curve, is estimated. To obtain a 2D section, all 1D velocity profiles inverted from each dispersion curve are interpolated along the seismic line.

Bohlen *et al*. (2004) developed a similar technique based on substantially overlapping arrays. They computed dispersion images on restricted receiver windows to account for local dispersion phenomena at the scale of the seismic line. Shear-wave profiles were then inverted in the 1D approximation. In the next section, we show that our approach uses this strategy but is also based on the summation principle that increases the signal-to-noise ratio and the resolution of the dispersion images.

In the light of these applications, there are still some unanswered questions (O'Neill 2004). The main problem lies in the assumption that the probed medium is horizontally layered (1D) around each receiver array. This is imposed by the popular 1D inverse-problem formulation used for data interpretation (Hermann 2002). In high-contrast media, where lateral velocity inhomogeneities are observed at the scale of the seismic line, S-wave velocity changes lead to phase variations in Rayleigh waves in the offset dimension. This phenomenon drastically alters the dispersion image, since it affects the local slopes of Rayleigh waves in the shot gather, and thus the phase-velocity dispersion properties. For example, Bodet *et al*. (2004, 2005) explained how a layer that dips at only a few degrees can significantly bias the surface-wave inversion.

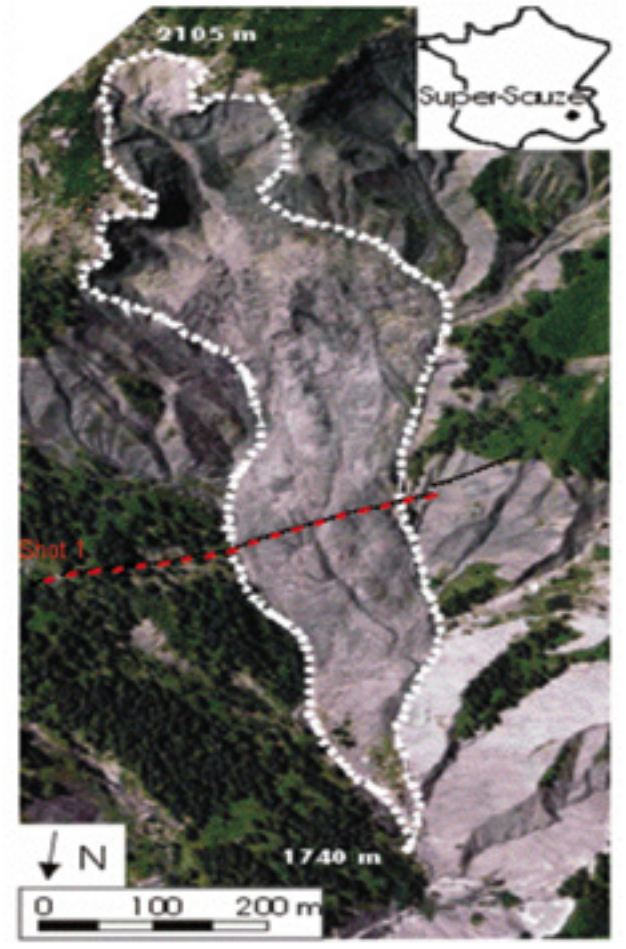

FIGURE 1
Location of Super-Sauze earthflow showing the seismic line; red stars indicate sources, black points indicate receivers.

In order to tackle this methodological problem, which is commonly encountered in many subsurface configurations, we propose a new algorithm for estimating the dispersion image. We extend the formulation of Park *et al*. (1998) by introducing a summation term, which sums over local dispersion images computed for different receiver gathers. The contribution of this algorithm is tested on synthetic examples before considering real data recorded on the Super-Sauze earthflow (France). This site was selected because seismic property changes, observed between the flanks and the centre of the earthflow, produce contrasting lateral velocity variations, thus providing good conditions to test the method. More details concerning the geological setting of this earthflow and related geophysical experiments can be found in Grandjean *et al*. (2005).

The Super-Sauze earthflow (Fig. 1) is a slow earthflow in the French Alps, situated in the Barcelonnette Basin on the left bank of the River Ubaye (Schmutz *et al*. 2000; Maquaire *et al*. 2001). It extends 820 m from its highest point at an elevation of 2105 m to its base at an elevation of 1740 m, with an average slope of 25°. It covers an area of about 17 hectares and is composed of Callovian-Oxfordian black marls, known as *Terres Noires*, with shades varying from black to a slightly blue grey. The surface is highly irregular, affected by plane fractures and surficial cracks (Malet *et al*. 2003), with several ravines in which crushed heterogeneous rocks and debris have accumulated.

The main seismic line was performed along a 335-m transverse profile perpendicular to the axis of the earthflow (white line in Fig. 1). 66 geophones placed at 5-m intervals were used and shots were fired using a detonating cord at 15-m intervals. Figure 2(a) shows the first seismic shot gather recorded on the eastern part of the profile. The strong velocity variations affecting the subsurface produce significant phase changes in the Rayleigh waves (Ra: Fig. 2a): on the eastern flank, which consists essentially of hard rocks, velocities are much higher that within the earthflow, which is composed mainly of unconsolidated and fractured rocks. From the data, these lateral velocity changes can be observed at trace no. 30, when the slope of the seismic Rayleigh waves decreases suddenly. Consequently, the dispersion image (Fig. 2b) computed from the entire set of traces is of poor quality because of destructive summations occurring during the transformation. The dispersion curve, defined as the points of maximum energy in the dispersion image, is therefore difficult to estimate.

Figure 2(c) shows the shear-wave velocity model obtained by using the inversion algorithm of Herrmann (2002). The initial model, i.e. the number of layers and their thicknesses, was esti-

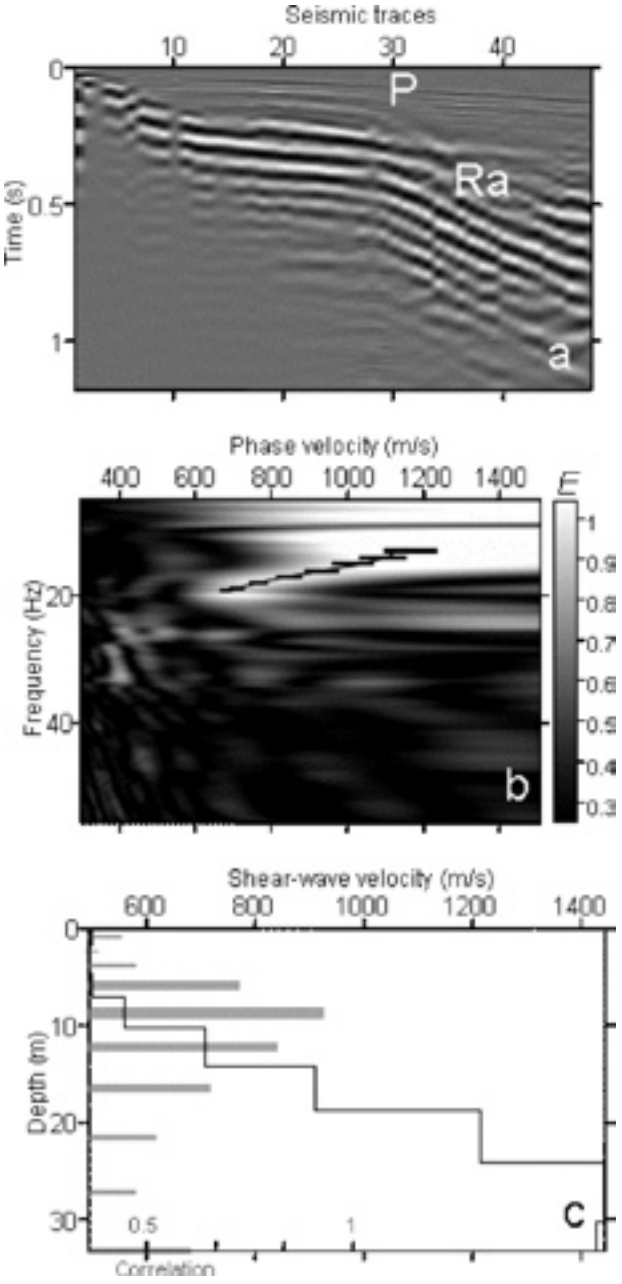

FIGURE 2

(a) Example of a seismic shot recorded on the Super-Sauze site, showing the P-waves (P) as first arrivals and Rayleigh waves (Ra) strongly affected by lateral velocity variations. (b) The corresponding dispersion image with the estimated dispersion curve (black line). This plot represents the normalized energy distributions E (equation (2)) of Rayleigh wave propagation modes. (c) Inverted shear-wave velocity profile. The correlation of inverted parameters, giving the reliability of velocities, is plotted in grey.

mated with respect to criteria defined by Orozco (2003). In particular, the number of layers was fixed at the number of points defining the observed dispersion curve. The thickness of the layers was estimated according to the empirical relationship between the wavelength λ and the depth of propagation $z = \lambda/2$ (Xia *et al*. 1999). Because of a lack of information in the lowest and highest frequency ranges, the correlation coefficient, computed with Herrmann's (2002) algorithm using inverted velocities, is weak for upper (0–5 m) and deeper (>20 m) layers. To increase the reliability of such models with respect to laterally heterogeneous seismic properties, we propose using seismic multifold acquisitions (2M-SASW: Multifold and Multichannel SASW) in order to redefine the computation of dispersion images in a more 'local' manner. For this, we take into account the dispersion relationship between the phase velocity and the frequency that occurs in a specific domain in the receiver line.

2M-SASW: THE LOCAL DISPERSION FORMULATION

For a given multichannel seismic record, dispersion images are commonly computed according to the method of Park *et al*. (1998). The dispersion image $E(\omega,c)$, showing the energy distribution of propagation modes in the angular frequency–phase velocity (i.e. ω–c) domain, is given by

$$E(\omega,c) = \int e^{-i\left(\Phi - \frac{\omega x}{c}\right)} \left(A(x,\omega) / \left| A(x,\omega) \right| \right) \mathrm{d}x , \qquad (1)$$

where Φ is the phase of the seismic signal, x is the receiver distance and $A(x,\omega)$ is the amplitude spectrum of the seismic signal.

For laterally contrasting media, the computation of the dispersion image has to be restricted to a narrow receiver distance window (x_1–x_2), for which the velocity field is assumed, as far as possible, to be laterally homogeneous. This assumption is necessary to ensure that the propagation of Rayleigh waves occurs mainly in a 1D stratified medium, which is the main hypothesis of our inverse problem. Assuming x_1 and x_2 are the limits of the receiver distance window (RDW), the local dispersion image defined in equation (1) is computed as

$$E(\omega,c)_{x_1}^{x_2} = \int_{x_1}^{x_2} e^{-i\left(\Phi - \frac{\omega x}{c}\right)} \left(A(x,\omega) / \left| A(x,\omega) \right| \right) \mathrm{d}x . \qquad (2)$$

This method, presented by Bohlen *et al.* (2004), was successfully applied to inverting Scholte-wave dispersion propagation below the sea-floor of the Baltic Sea. However, in that study, the dispersion images were computed from only a single shot gather and therefore with a minimum number of traces. In order to improve the signal-to-noise ratio of the local dispersion image, we tried to use additional traces obtained from the next shots, provided that these traces were within the same RDW. This was achieved by using a multifold acquisition procedure. If a series of shots are recorded along the same profile, we can compute new quantities, $E_L(s,\omega,c)_{x_1}^{x_2}$, representing the local dispersion diagrams related to each shot:

$$E_L(s,\omega,c)_{x_1}^{x_2} = \int_{x_1}^{x_2} e^{-i\left(\Phi - \frac{\omega x}{c}\right)_s} \left(A(s,x,\omega) / \left| A(s,x,\omega) \right| \right) \mathrm{d}x , \qquad (3)$$

where s is the shot distance. This method is an extension of the one proposed by Hayashi and Suzuki (2004) for computing dispersion images and is based on common midpoint (CMP) correlations. Using the summation principle as a technique for increasing the signal-to-noise ratio, each dispersion image (equation (3)) computed in the same RDW can be stacked in order to compute the local dispersion image stack (LDS), i.e.

$$E_L(\omega,c)_{x_1}^{x_2} = \iint_{x_1}^{x_2} e^{-\left(\frac{x-x_c}{\sigma}\right)^2} \left(A(s,x,\omega)/\left|A(s,x,\omega)\right|\right) \mathrm{d}x\mathrm{d}s \,. \qquad (4)$$

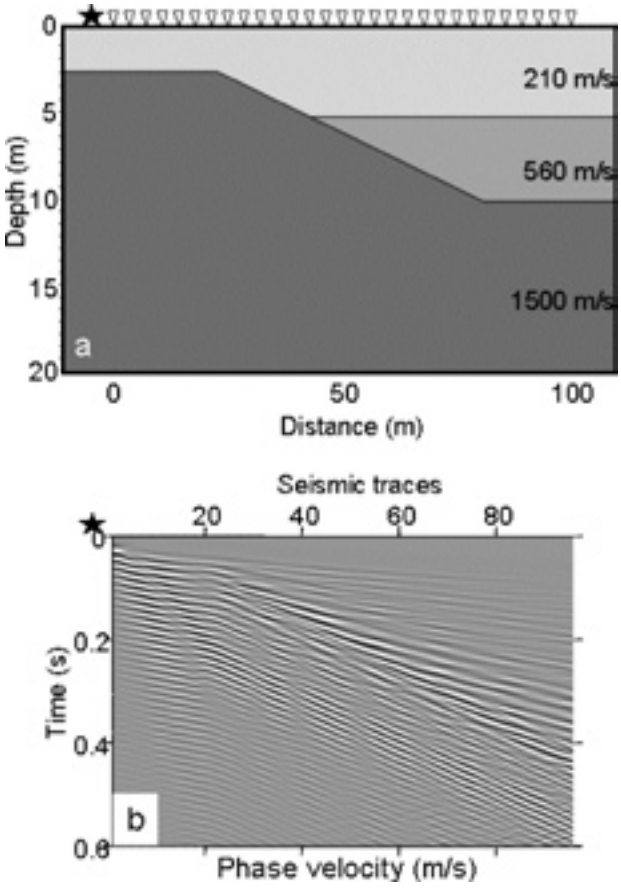

FIGURE 3

(a) 2D elastic model (only shear-wave values are indicated) used to compute synthetic seismograms: sources and receivers are set regularly along the top every 10 m and 1 m, respectively. (b) Synthetic seismic shot computed according to the model of Fig. 3(a) (X_{shot} = 10 m).

To illustrate this approach, we tested equation (4) on a synthetic case. The elastic model is composed of three layers of different elastic properties:

- Layer #1: V_P=420 m/s, V_S=210 m/s, ρ=1800 kg/m^3;
- Layer #2: V_P=1120 m/s, V_S=560 m/s, ρ=1900 kg/m^3;
- Layer #3: V_P=2100 m/s, V_S=1500 m/s, ρ=2000 kg/m^3,

producing a 2D geometry as shown in Fig. 3(a). The finite-difference time-domain (FDTD) scheme used to compute seismograms was adapted from Virieux (1986), Levander (1988) and Juhlin (1995), and is based on the stress–velocity wave equation in two dimensions. Equations of motion are differentiated and solved using a 2D staggered finite-difference grid (Virieux 1986; Levander 1988). Boundary conditions are classically defined to model a semi-infinite space, satisfying the free-surface conditions at depth z = 0. The other boundaries at the grid periphery are coded to satisfy the Clayton–Engquist (1977) absorbing conditions. A spatially localized source is introduced with a second Gaussian derivative function of stress components, using the source insertion principle of Alterman and Karal (1968). Sources and receivers were placed along the horizontal x-axis between 10 m and 90 m, every 10 m and 1 m, respectively.

Figure 3(b) shows a synthetic seismic shot, representing the vertical displacement generated by a source point located at x = 0 m, z = 0 m, and recorded at receiver points spread over the

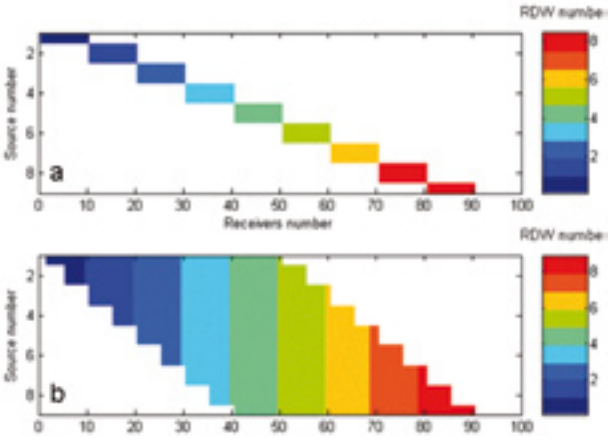

FIGURE 5

Source–receiver plot showing how the traces are distributed over RDWs: (a) in the case of dispersion image, (b) in the case of a local dispersion stack.

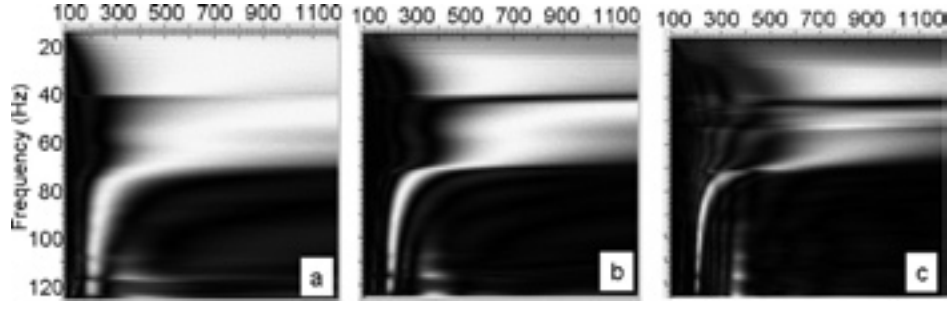

FIGURE 4

Dispersion images computed from traces of the synthetic shot gather (Fig. 3b) with offset less than (a) 6 m, (b) 12 m and (c) 24 m.

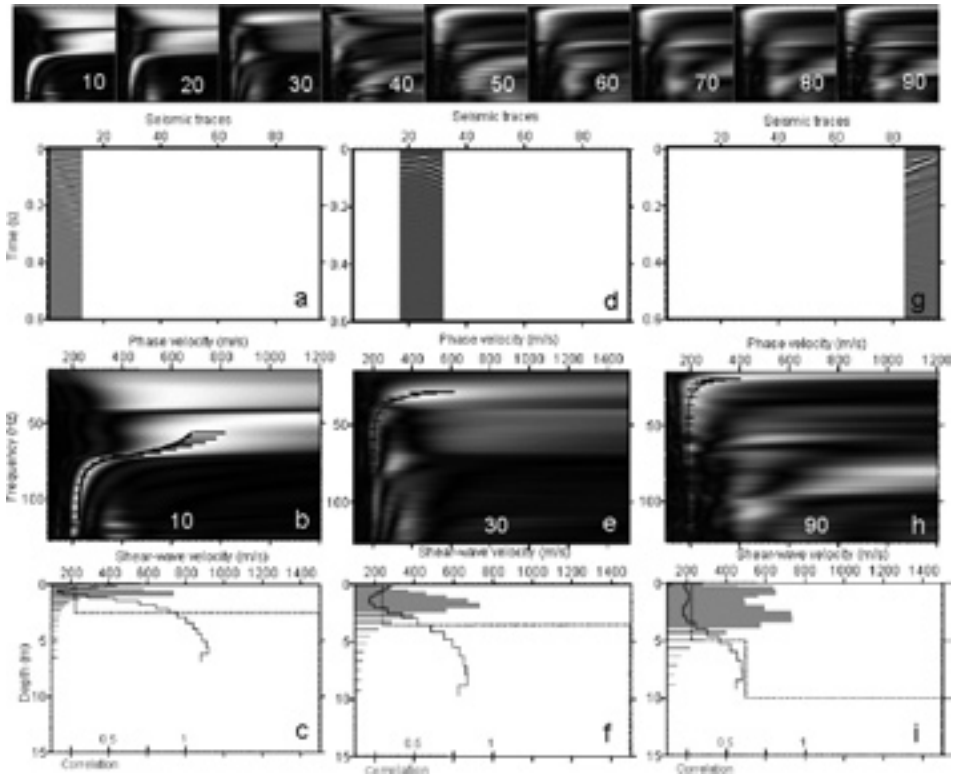

FIGURE 6
Top row: dispersion images for the whole set of synthetic shots (source position is indicated by white numbers). Selected traces (a), (d), (g) used for computing the dispersion images (b), (e), (h); inverted shear-wave velocity profiles (c), (f), (i) for the shots fired at 10 m (a), 30 m (d) and 90 m (g). Dotted lines represent the *z*-gradient of the local (1D) shear-wave velocity.

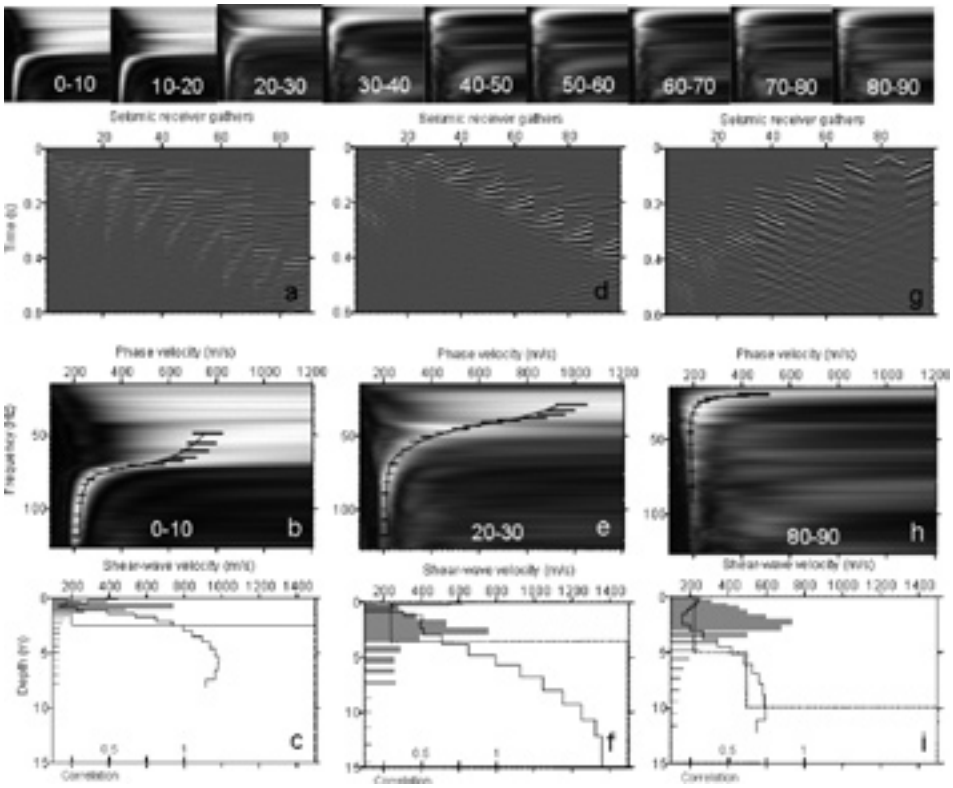

FIGURE 7
Top row: dispersion images for the whole set of receiver gathers (receiver gathering window is indicated). Selected gathers (a), (d), (g) used for computing the dispersion images (b), (e), (h) and inverting the shear-wave velocity profiles (c), (f), (i) for the receivers between 0 and 10 m (a), 20 and 30 m (d), 80 and 90 m (g). Dotted lines represent the *z*-gradient of the local (1D) shear-wave velocity.

surface. The dispersion images shown in Fig. 4(a,b,c) were computed according the traditional algorithm of Park *et al*. (1998) for offset windows of 6 m, 12 m and 24 m length, respectively. These three cases show the impact of the number of traces considered in the computation (6, 12 or 24 in this case) on the quality of the dispersion image: too few traces lead to a lack of reso-

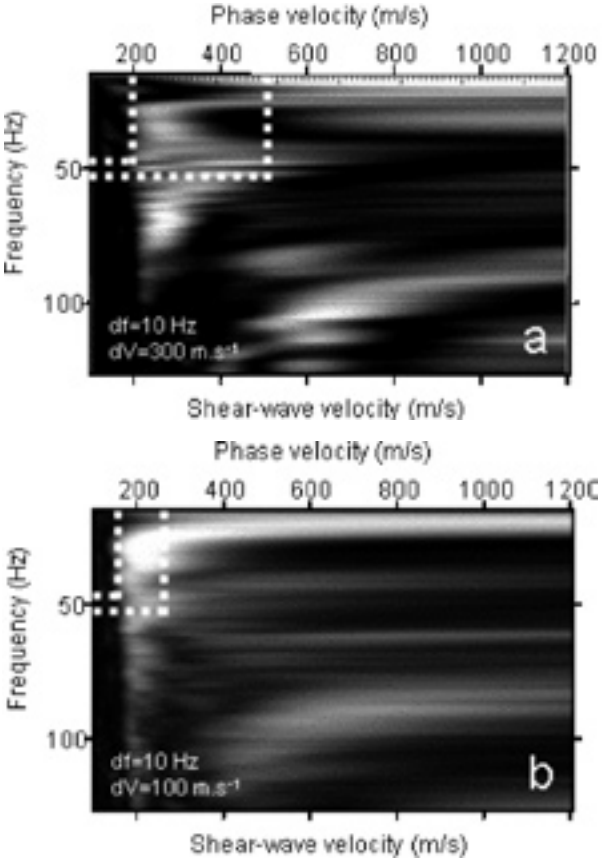

FIGURE 8

(a) Dispersion image computed with the traditional method (equation (2)) and corresponding to the image no. 40 in Fig. 6. (b) Local dispersion stack computed according to the 2M-SASW method (equation (4)) and corresponding to the stack no. 40-50 in Fig. 7. The width of the energy band for a frequency bandwidth of 10 Hz is compared in term of spreading of the phase velocity.

lution (Fig. 4a), while too many traces mix the effects of lateral velocity changes (Fig. 4c). A good compromise in this case is reached for an offset window length of 10 m (Fig. 4b): dispersion properties of the first part of the model, assumed to be 1D, are only considered when the number of traces is sufficiently high to produce a good signal-to-noise ratio image. For the next computations, we follow this statement by choosing the RDW so that $|x_2 - x_1| = 10$ m. Figure 5 illustrates the impact of equations (2) and (4) on the traces selected for computing dispersion images and LDSs, respectively. In the first case, ten traces are used to compute the dispersion image corresponding to a particular shot gather with a limited offset window. In the second case, a large number of traces of different offsets are used to compute several dispersion images that are finally stacked over the same RDW.

Figures 6 and 7 compare the dispersion images of synthetic data and show three inverted shear-wave velocity profiles for both the MASW (shot gather) and 2M-SASW (receiver gathers) approaches. A series of dispersion images computed from nine shot gathers (Fig. 6) or nine receiver gathers (Fig. 7) are shown in the top row of each figure. We note that the quality of images computed from shot gathers (top row of Fig. 6) are strongly affected by the lateral velocity changes. This is particularly clear for shots 30 to 50, where a poor signal-to-noise ratio is observed, making it difficult to identify the fundamental mode. In contrast, LDSs computed from receiver gathers (top row of Fig. 7) are of good quality and show a continuous evolution of dispersion characteristics between gathers 0–10 and 80–90, in good agreement with the lateral velocity changes in the 2D synthetic velocity model. Trace gathers, dispersion images and inverted models are also presented for the first (Fig. 6a–c and Fig.7a–c), the middle (Fig.6d–f and Fig.7df) and the last (Fig.6g–i and Fig.7g–i) shot and receiver gathers, respectively. The two approaches have almost similar results when considering the first and the last parts of the model, although the sharpness of the dispersion images is better when using 2M-SASW. For the middle part of the model, only the LDS can clearly identify the fundamental mode, making 2M-SASW better adapted. This has a drastic impact on the inversion results, and in the three cases, the 2M-SASW method enables a deeper characterization of the shear-wave velocity field. This is particularly true when comparing Figs 6(f) and 7(f).

Another comparison between both methods is shown in Fig. 8. The phase-velocity spreading (dV) is estimated from the energy band corresponding to a frequency bandwidth of 10 Hz (df) and centred on 50 Hz. According to Zhang *et al*. (2004), the ratio df/dV is a good indicator of the resolution of dispersion spectra. Figure 8 clearly shows that LDS (equation (4)) provides a better resolution, with a df/dV ratio of around 0.10 m^{-1}, than the traditional dispersion image computation, with a df/dV ratio of around 0.03 m^{-1} (equation (2)).

Several authors have pointed out the impact of near-field effects on the quality of dispersion curves computed from two-station measurements (Sànchez-Salinero 1987; Tokimatsu 1995; Ganji *et al*. 1998). Regarding MASW, the problem is also mentioned by O'Neill and Matsuoka (2005) and Strobbia and Foti (in press). As suggested by these authors, such effects can be attributed either to direct body waves, which are more influential in the vicinity of the source, or to the inappropriateness of the plane-wave model with the cylindrical spreading of Rayleigh waves from a point source. These remarks should lead to near-offsets being discarded and only larger offsets being considered. On the other hand, we have already mentioned that, in highly laterally contrasted media, considering large offsets affects the lateral resolution of dispersion images (Fig. 8). Minimizing these two effects is, however, taken into account in the 2M-SASW approach: (i) near offsets can be neglected in order to suppress near-field effects; (ii) dispersion images are computed in narrow-offset windows and stacked for different source positions in order to restrict velocity inhomogeneities in the RDW and to increase the signal-to-noise ratio. The resolution of the resulting LDSs is thus preserved with minimized near-offset effects.

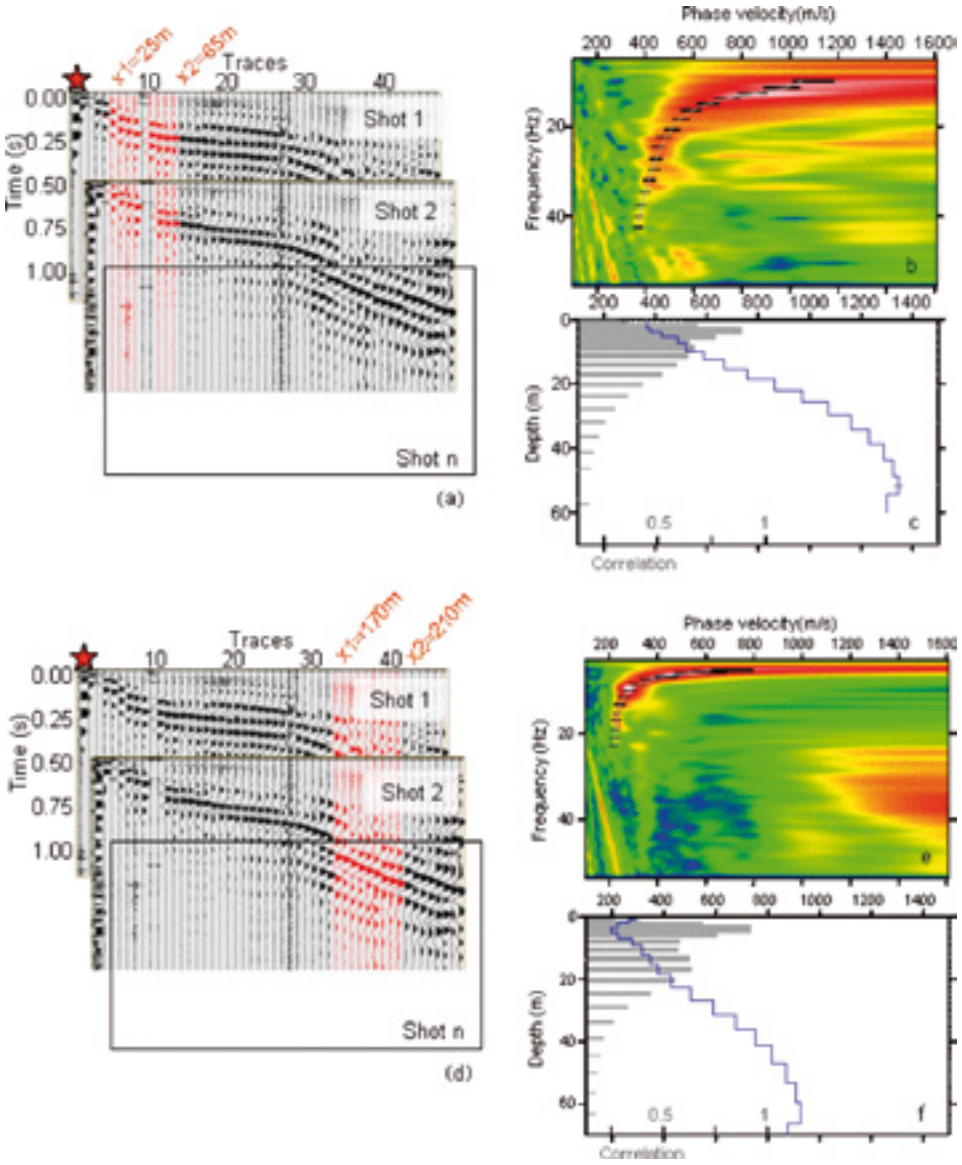

FIGURE 9
Example of trace selection on 2 consecutive shots for a distance window ranging from (a) 25 to 65 m and (d) 170 to 210 m, respectively. Local dispersion stacks corresponding to (a) and (d) are represented in (b) and (e), respectively. Shear-wave velocity profiles after dispersion curves have been inverted are plotted in (c) and (f).

APPLICATION TO SUPER-SAUZE

For the Super-Sauze data, the RDW was set at 40 m. Nine traces were thus selected for each receiver gather leading to the calculation of the LDS. Figure 9 shows, for the first two shots, the traces selected for two RDWs ranging from 25 m to 65 m and 170 to 210 m. This RDW of 40 m consists of ten traces, as in the synthetic case considered above. As can be seen, the slopes of the Rayleigh waves in the shot gather are very different for these two RDWs, thus rendering the conventional computation of dispersion images inefficient. The length of the RDW is thus an important parameter that has to be estimated according to the minimum trace distance in which the slope of Rayleigh waves varies. A comparison between Fig. 2(b) and Figs 9(b) and 9(e) shows the contribution of the LDS in the estimation of the dispersion curve: because they are computed in a restricted distance window, the dispersion properties are more accurately defined than in the traditional way. The inversion of the local dispersion was then carried out using Hermann's (2002) programs. Figure 9(b, e) shows the observed and calculated dispersion curves corresponding to the two RDWs defined above. The resulting shear-wave velocity models are also shown with the correlation of inverted parameters. In this example, the velocities playing a dominant role in the Rayleigh-wave dispersion range from 0 to around 40 m, while they were defined down to 30 m with the conventional technique (Fig. 2c). Finally, we note that the two models in Fig. 9 are also very different since they refer to dispersion processes occurring in two different places along the profile: the two RDWs here are related to the flank of the landslide and the earthflow.

In order to construct a 2D shear-wave velocity image of the earthflow, LDSs were computed for each RDW, moving incrementally from 0–40 m to 300–340 m. Following the same

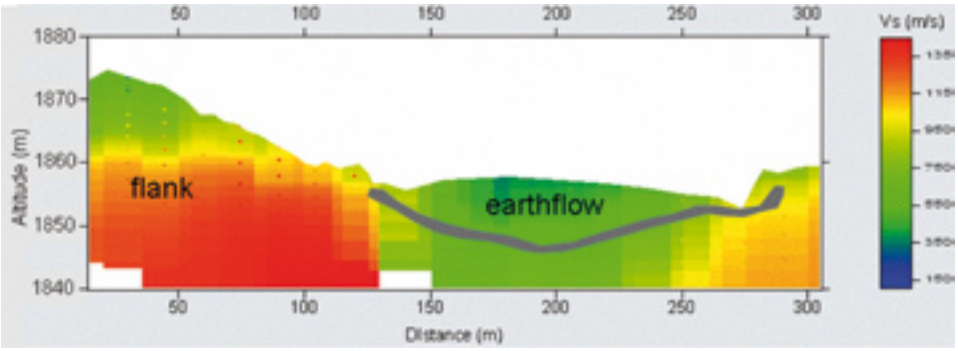

FIGURE 10
2D shear-wave velocity section after shear-wave profiles inverted from local dispersion stacks have been interpolated along the seismic line. The grey line represent the earthflow basement as described by Malet (2003).

processing protocol, all LDSs were inverted and interpolated along the seismic line. Figure 10 shows the results of this work, by presenting the final shear-wave velocity cross-section of the site. The flanks and the earthflow can be easily distinguished by the highest (900–1400 m/s) and the lowest (400–900 m/s) velocity values, respectively. In the earthflow area, a lower-velocity zone (150–350 m/s) indicates the active part mentioned by Malet (2003), who identified its basement. This 2D shear-wave velocity section, computed using 2M-SASW, has shown good agreement with other geophysical results available at the Super-Sauze site. The significant improvements offered by 2M-SASW in terms of the signal-to-noise ratio of the dispersion images has opened the way to a possible combination of different geophysical images. Using the P-wave velocity and electrical tomographies, in addition to the S-wave velocity image of Fig.10, it was possible to refine the global diagnosis by identifying the earthflow geomechanical structures, as presented by Grandjean *et al*. (2005).

CONCLUSIONS

The aim of our study was to extend the SASW method with a multifold acquisition, and to propose the 2M-SASW (Multifold and Multichannel - Spectral Analysis of Surface Waves) method as a new technique for processing dispersion images in highly laterally contrasted media. This work consists of redefining the computation of dispersion images in a more 'local' manner. This appears to be suitable when media are laterally heterogeneous, because S-wave velocity changes lead to phase variations in Rayleigh waves in the offset dimension. This phenomenon can drastically alter the dispersion image since it affects the local slopes of Rayleigh waves in the shot gather and thus their phase-velocity dispersion properties. The proposed 2M-SASW method consists of gathering traces within a restricted receiver window for a series of shots, computing the related local dispersion images and then stacking them in order to improve the signal-to-noise ratio to obtain the local dispersion stack (LDS). The inversion of the dispersion curve observed on the LDS is based on a classical 1D model and leads to the estimation of the local shear-wave velocity profiles. All velocity profiles are finally interpolated along the seismic line to produce a 2D section. This method was tested on synthetic data to demonstrate its contribution compared to the traditional SASW technique. An application to the Super-Sauze earthflow was presented and confirmed that 2M-SASW is well suited to inverting the shear-wave velocity from Rayleigh-wave dispersion when high-contrast media are considered.

REFERENCES

Alterman Z. and Karal F.C. 1968. Propagation of elastic waves in layered media by finite-difference methods. *Bulletin of the Seismological Society of America* **58**, 367–398.

Bodet L., Abraham O., Bitri A., Leparoux D. and Côte P. 2004. Effect of dipping layers on seismic surface waves profiling: a numerical study. *Proceedings of Symposium on the Application of Geophysics to Engineering and Environmental Problems*,

Bodet L., van Wijk K, Bitri A., Abraham O, Côte P. Grandjean G. and Leparoux D. 2005. Surface wave dispersion inversion when the 1D assumption breaks down. 1st General Assembly of the European Geosciences Union, Vienna, Austria, Expanded Abstracts, 24–29.

Bohlen T., Kugler S., Klein G. and Theilen F. 2004. 1.5D inversion of lateral variation of Scholte-wave dispersion. *Geophysics* **69**, 330–334.

Clayton R. and Engquist B. 1977. Clayton-Engquist A1 boundary conditions. *Bulletin of the Seismological Society of America* **67**, 1529–1540.

Ganji V., Gucunski N. and Nazarian S. 1998. Automated inversion procedure for spectral analysis of surface waves. *Journal of Geotechnical and Geoenvironmental Engineering* **124**, 757–770.

Grandjean G. in press. A seismic multi-approach method for characterizing contaminated sites. *Journal of Applied Geophysics* (in press)

Grandjean G., Malet J.P., Bitri A. and Meric O. 2005. Geophysical data fusion by fuzzy logic for imaging earthflow mechanical behaviour. 11th European Meeting of Environmental and Engineering Geophysics (EAGE), Palermo, Italy,

Hayashi K. and Suzuki H. 2004. CMP cross-correlation analysis of multi-channel surface-wave data. *Exploration Geophysics* **35**, 7–13.

Herrmann R.B. 2002. *Computer programs in seismology*. Department of Earth and Atmospheric Sciences, Saint Louis University.

Juhlin C. 1995. Finite-difference elastic-wave propagation in 2D heterogeneous transversely isotropic media. *Geophysical Prospecting* **43**, 843–858.

Levander A.R. 1988. Fourth-order finite-difference P-SV seismograms. *Geophysics* **53**, 1425–1436.

Lin C.-P. and Chang T.-S. 2004. Multi-station analysis of surface wave dispersion. *Soil Dynamics and Earthquake Engineering* **24**, 877–886.

Malet J.-P. 2003. *Les 'glissements de type écoulement' dans les marnes noires des Alpes du Sud. Morphologie, fonctionnement et modélisation hydro-mécanique*. PhD thesis, Louis Pasteur University, Strasbourg, France.

Malet J.-P. and Maquaire O. 2003. Black marl earthflows mobility and long-term seasonal dynamic in southeastern France. In: *Proceedings of the International Conference on Fast Slope Movements: Prediction and Prevention for Risk Mitigation* (ed. L. Picarelli), Napoli, Italy, pp. 333–340. Patron Editore, Bologna.

Maquaire O., Flageollet J.-C., Malet J.-P., Schmutz M., Weber D., Klotz S., Albouy Y., Descloîtres M., Dietrich M., Guérin R. and Schott J.-J. 2001. Une approche multidisciplinaire pour la connaissance d'un glissement-coulée dans les marnes noires du Callovo-Oxfordien (Super-Sauze, Alpes de Haute-Provence, France. *Revue Française de Géotechnique*, **95-96**, 15–31.

Miller R.D., Xia J., Park C.B. and Ivanov J. 1999. Multichannel analysis of surface waves to map bedrock. *The Leading Edge* **18**, 1392–1396.

Nazarian S., Stokoe K.H. and Hudson W.R. 1983. Use of spectral analysis of surface waves method for determination of moduli and thickness of pavement system. *Transportation Research Record* **930**, 38–45.

O'Neill A. 2004. Some pitfalls associated with dominant higher-mode inversion. In: *Proceedings of the 8th International Symposium on Recent Advances in Exploration Geophysics* (RAEG2004), Kyoto University, pp. 48–55.

O'Neill A., Dentith M. and List R. 2003. Full-waveform P-SV reflectivity inversion of surface waves for shallow engineering applications. *Exploration Geophysics* **34**, 158–173.

O'Neill A. and Matsuoka T. 2005. Dominant higher surface-wave modes and possible inversion pitfalls. *Journal of Engineering and Environmental Geophysics* (*EEGS*) **10**, 185–201.

Orozco C. 2003. *Inversion method for spectral analysis of surface waves* (*SASW*). PhD thesis, Georgia Institute of Technology, Georgia, USA.

Park C.B., Miller R.D. and Xia J. 1998. Imaging dispersion curves of surface waves on multi-channel record. 68th SEG Meeting, New Orleans, USA, Expanded Abstracts, 1377–1380.

Park C.B., Miller R.D. and Xia J. 1999a. Multimodal analysis of high frequency surface waves. *Proceedings of Symposium on the Application of Geophysics to Engineering and Environmental Problems '99*, 115–121.

Park C.B., Miller R.D. and Xia J. 1999b. Multichannel analysis of surface waves. *Geophysics* **64**, 800–808.

Rix G.J., Lai C.G. and Foti S. 2001. Simultaneous measurement of surface wave dispersion and attenuation curves. *Geotechnical Testing Journal* **24**, 350–358.

Sànchez-Salinero I. 1987. *Analytical investigation of seismic methods used for engineering applications*. PhD dissertation, University of Texas at Austin.

Schmutz M., Albouy Y., Guérin R., Maquaire O., Vassal J., Descloîtres M. and Schott J.-J. 2000. Contribution of electrical and TDEM methods employed separately and combined to Super-Sauze flowslide knowledge. *Surveys in Geophysics* **21**, 371–390.

Strobbia C. and Foti S. In press. Multi-offset phase analysis of surface wave data (MOPA). *Journal of Applied Geophysics* (in press)

Tokimatsu K. 1995. Geotechnical site characterisation using surface waves. In: *Proceedings of 1st International Conference on Earth Geotechnical Engineering* (ed. K. Ishihara), pp. 1333–1368. Balkema, Rotterdam.

Virieux J. 1986. SH-wave propagation in heterogeneous media: Velocity-stress finite-difference method. *Geophysics* **49**, 1933–1957.

Xia J., Miller R.D. and Park C.B. 1999. Configuration of near surface shear wave velocity by inverting surface wave. *Proceedings of Symposium on the Application of Geophysics to Engineering and Environmental Problems '99*, pp. 95–104.

Yaramanci U. 2004. Seismic surface waves in Near Surface Geophysics. *First Break* **22**(November), 4–6.

Zhang S.X., Chan L.S. and Xia J. 2004. The selection of field acquisition parameters for dispersion images from multichannel surface wave data. *Pure and Applied Geophysics* **161**, 185–201.